Meteoritics & Planetary Science 35, 1259-1267 (2000)

Image-intensified video results from the 1998 Leonid shower: I. Atmospheric trajectories and physical structure

M. D. CAMPBELL[1*], P. G. BROWN[1], A. G. LEBLANC[2†], R. L. HAWKES[2], J. JONES[1], S. P. WORDEN[3] AND R. R. CORRELL[4]

[1]Department of Physics and Astronomy, University of Western Ontario, London, Ontario N6A 3K7, Canada
[2]Physics Department, Mount Allison University, 67 York Street, Sackville, New Brunswick E4L 1E6, Canada
[3]Headquarters United States Air Force, 1480 Air Force Pentagon, Washington, D.C. 20330-1480, USA
[4]Headquarters United States Air Force Space Command and NASA Headquarters, 300 E St. SW, Washington, D.C. 20546, USA
[†]Present address: Department of Astronomy and Physics, Saint Mary's University, Halifax, Nova Scotia B3H 3C3, Canada
*Correspondence author's e-mail address: mdcampbe@julian.uwo.ca

(Received 2000 March 16; accepted in revised form 2000 July 24)

Abstract–Two-station electro-optical observations of the 1998 Leonid shower are presented. Precise heights and light curves were obtained for 79 Leonid meteors that ranged in brightness (at maximum luminosity) from +0.3 to +6.1 astronomical magnitude. The mean photometric mass of the data sample was 1.4×10^{-6} kg. The dependence of astronomical magnitude at peak luminosity on photometric mass and zenith angle was consistent with earlier studies of faint sporadic meteors. For example, a Leonid meteoroid with a photometric mass of ~1.0×10^{-7} kg corresponds to a peak meteor luminosity of about +4.5 astronomical magnitudes. The mean beginning height of the Leonid meteors in this sample was 112.6 km and the mean ending height was 95.3 km. The highest beginning height observed was 144.3 km. There is relatively little dependence of either the first or last heights on mass, which is indicative of meteoroids that have clustered into constituent grains prior to the onset of intensive grain ablation. The height distribution, combined with numerical modelling of the ablation of the meteoroids, suggests that silicate-like materials are not the principal component of Leonid meteoroids and hints at the presence of a more volatile component. Light curves of many Leonid meteors were examined for evidence of the physical structure of the associated meteoroids: similar to the 1997 Leonid meteors, the narrow, nearly symmetric curves imply that the meteoroids are not solid objects. The light curves are consistent with a dustball structure.

INTRODUCTION

Understanding the physical structure and chemical composition of shower meteoroids is important to understanding these same quantities in the associated parent comets. The height at which meteoroids ablate, for a given mass and velocity, is a particularly good diagnostic measure of the chemical composition of meteoroids. The beginning height is particularly revealing: the boiling point and density of the meteoroid places an upper bound on the height at which ablation may begin. The vast majority of sporadic and shower meteors have beginning heights (as measured by two-station image intensified video techniques) in the range from 90 to 120 km (Hawkes and Jones, 1980; Hapgood *et al.*, 1982; Hawkes *et al.*, 1984; Sarma and Jones, 1985; Ueda and Fujiwara, 1995). However, previous two-station studies of Leonid meteors have found beginning heights for a few bright fireballs as high as 160 km (Fujiwara *et al.*, 1998) to 200 km (Betlem *et al*., 1999). One possible interpretation of these observations is that the meteoroids are much more volatile than conventional theory suggests. This would be consistent with the suggestion of Steel (1998) that there may be a significant volatile component in Leonid meteoroids.

It is also possible to impose constraints upon the physical structure of Leonid meteors from their light curves. By comparing the shape of the light curve produced from classical theoretical models of ablation to the observed light curve, some possible ablation mechanisms can be ruled out. Evidence to date suggests that most shower meteoroids are dustballs, that is, collections of solid grains (Jacchia, 1955; Verniani, 1969), probably bound with a more volatile "glue" (Hawkes and Jones, 1975; Campbell, 1998; Campbell *et al.*, 1999). This volatile component probably evaporates completely before the onset of light production, and each solid grain then ablates individually. This is consistent with observations of other small meteors (Beech, 1984). Large meteors show evidence of gross fragmentation consistent with a solid core of material that breaks up as they ablate (*e.g.*, Ceplecha *et al.*, 1993, 1998).

Although the dustball model has been supported in a number of studies over the past several decades, that is not to say that difficulties do not persist (Fisher *et al*., 2000). In particular, it appears that faint meteors have very little spread of constituent grains along the meteor trail (Shadbolt and Hawkes, 1995), which either sets limits on possible grain-size distribution or implies that the dustball model itself may require revision.

As well as the absolute values of the beginning heights, the mass dependence of the beginning and ending heights, and the trail lengths, can be used to support a specific dustball ablation model. For example, if, as suggested above, for smaller meteoroids, grain release occurs prior to intensive ablation of the grains themselves, one would expect that heights and trail lengths would become largely independent of mass. Such a model was found to be consistent with observations of meteoroids of cometary origin from the Perseid (Hapgood *et al.*, 1982) and Draconid (Beech, 1986) showers.

The height and mode of ablation is important for understanding the atmospheric effects caused by these meteors and may be important for proper modeling of the interaction between meteoroids and spacecraft (Hawkes *et al*., 1998; Correll *et al*., 1999). In this paper, we present results from a dual-station observational study of the 1998 Leonid shower, with particular attention to the atmospheric trajectory over which ablation takes place and the implications for physical structure.

EQUIPMENT AND DATA COLLECTION

During the 1998 Leonid campaign in Mongolia, data were collected with a total of 10 image intensified video cameras over the four nights November 15–18 U.T., inclusive. Additional cameras were located in Australia and operated in conjunction with a multifrequency meteor radar: data from those systems will be reported separately. Nine of the cameras used in Mongolia employed Cohu 4910 series CCD video cameras, which record at NTSC rates (30 interlaced video frames per second). Each of these was lens-coupled to an image intensifier: six of the image intensifiers were Generation II and three were Generation III image intensifiers. Generation III image intensifiers use a photocathode that results in an enhancement of sensitivity in the near infrared. The Generation II image intensifiers used in this work employed a photocathode with an S-20 spectral response, which approximates that of the human eye. In both cases, the total spectral response of the system extends from ~340 to 870 nm; although, in the case of the Generation III systems, the response is stronger in the red and near-infrared regions than for the Generation II systems.

Five cameras, including three Generation II, one Generation III, and one ISIT (the video from which has not yet been analysed and is not presented in this paper) were located at the Khureltogoot observatory in Mongolia (107.0517° E, 47.8653° N). C-mount objective lenses with focal lengths from 25 to 75 mm were used, producing fields of view ranging from 35° to 9°, and a maximum limiting stellar magnitude on the most sensitive systems of nearly +9M. The limiting photometric mass for the most sensitive cameras was ~2×10^{-8} kg for Leonid meteors, as calculated from the integrated luminosity of the entire meteor. The other five, three Generation II cameras and two Generation III, were located at a remote site 54.6 km away (106.7458° E, 47.4197° N). One camera at each station followed the radiant, and the other four were used in triangulation. Problems on the peak night (1998 November 17) meant that one pairing of cameras produced no useful two-station meteors. The majority of two-station meteors reported here were recorded on the two cameras that used the 25 mm focal length lenses, and therefore, had the widest fields of view. All data were recorded on VHS or S-VHS videotape in SP record mode.

A total of 1509 meteors were analyzed, of which 316 were designated Leonid meteors (using radiant and relative velocity discriminators). Whereas approximate meteor trajectories can be obtained for shower meteors using single-station results, the most precise heights are obtained by triangulation from two stations. These yielded 81 double-station Leonid meteors, of which 79 yielded precision results and are described here. The results for individual meteors are presented in Table 1.

In the campaign, each camera system had a letter designation. The 79 meteors reported here were all a result of pairing of an observation from camera A with one from camera F, or a meteor-pairing between camera J and camera K. The orientation and performance characteristics of these four cameras are given in Table 2.

ANALYSIS PROCEDURES

MeteorScan software developed by P. Gural was used for automated detection of meteors from the video records, with subsequent human confirmation. In a few cases, human observers were used in place of MeteorScan for visual detection. It is estimated that MeteorScan, under optimal operation, detects ~70% of the meteors that would be detected by a careful human observer, with most of the missed meteors near the limiting magnitude of the system.

Following confirmation, the analog meteor video records were digitized using a SCION LG-3 card to $640 \times 480 \times 8$-bit resolution. The digital image processing package NIH Image 1.62 (with the addition of custom meteor macro routines) was used to perform digital image processing and measurement on the resulting stacks of meteor images.

At least twice, for each camera position, a number (typically 12 to 18) of reference stars were measured to establish positional and photometric calibrations. The positional calibrations employed a "plate constants" approach (Wray, 1967; Marsden, 1982; Hawkes *et al.*, 1993) to fit actual pixel coordinates to those expected for an ideal (distortion free) plate coordinate system. Seven terms, including those to cubic, were used; cross terms were found to have no significant effect and were neglected. The same calibration stars were used for the photometric calibration using the technique described by Hawkes *et al.* (1993) and Fleming *et al.* (1993) and employed in the light curve study by Campbell *et al.* (1999).

The procedures for triangulation of television meteor data have been described in detail elsewhere (Hawkes *et al.*, 1993) and will only be briefly summarized here. The technique is not significantly different from the procedures developed for two-station photographic reductions (Wray, 1967; Ceplecha, 1987).

First, a best-fit line is found for the meteor on each camera, using all points on the meteor's trajectory: this will tend to eliminate small errors in the positional measurements. The geometry of the two-station analysis is indicated in Fig. 1. Here $\boldsymbol{d}$ is a baseline vector pointing from station 1 to station 2. Taking the cross product of vectors to the corrected first and last points ($\boldsymbol{b}$ and $\boldsymbol{e}$ in Fig. 1) gives a vector normal ($\boldsymbol{n}$) to the plane containing the meteor as viewed from each site. The cross product of the normals of these planes must then lie along the trail of the meteor, and the apparent radiant can thus be determined. The orientation of the vector $\boldsymbol{r}$, in the direction of the meteor, can easily be obtained by converting to Earth-based coordinates.

Once the radiant vector is obtained, one can set up vector equations with three scalar parameters to be determined from the three components of the vector equation. The following equations (with reference to the notation of Fig. 1) constitute the systems solved in our triangulation routine:

$$c_{b1}\hat{\boldsymbol{b}}_1 = \boldsymbol{d} + c_{e2}\hat{\boldsymbol{e}}_2 + c_{r12}\hat{\boldsymbol{r}}$$
$$c_{e1}\hat{\boldsymbol{e}}_1 = \boldsymbol{d} + c_{b2}\hat{\boldsymbol{b}}_2 + c_{r21}\hat{\boldsymbol{r}}$$

For example, c_{b1} will represent the range from station 1 to the apparent beginning point of the meteor as viewed from that station. The other scalar parameters have a similar interpretation. One strength of this approach is that it is not necessary to assume any common point (as viewed from both stations) and, indeed, the solution yields the offset of the apparent beginning point from one station compared to that as viewed from the second station.

A conversion of the radiant vector to geocentric coordinates yields the zenith angle. The time information provided by the video frame rate can be used to determine velocities. Heights can be calculated once the range and angle to any specific meteor point is known. Because the analysis is done in Cartesian coordinates fixed on station one, a small correction is applied for the curvature of the Earth in determining the vertical heights of the meteors.

Meteor magnitudes are determined from the photometric procedures described by Hawkes *et al.* (1993) and Fleming *et al.*

TABLE 1. Double-station results for individual meteors.*

Cam	Day	Time (U.T.)	nf	Mag	Mass (kg)	RA	Dec	cos(*z*)	*Hf* (km)	*Hb* (km)	*He* (km)	*Hl* (km)	ΔL (km)
A,F	17	19:23:39	8	5.48	6.1×10^{-8}	153.0	20.6	0.59	107.55	–	98.32	98.32	15.58
A,F	17	19:25:17	3	5.22	5.0×10^{-8}	156.6	15.8	0.52	112.45	112.45	–	108.09	8.56
A,F	17	19:29:46	5	6.05	1.5×10^{-8}	137.2	31.9	0.82	108.60	108.60	101.32	101.32	8.84
A,F	17	19:36:15	15	3.43	9.0×10^{-7}	153.1	19.4	0.61	119.35	119.35	–	100.76	30.57
A,F	17	19:39:56	19	3.11	1.3×10^{-6}	153.4	19.6	0.62	125.60	–	–	100.03	41.36
A,F	17	19:41:23	8	4.70	1.3×10^{-7}	152.2	20.4	0.64	107.42	107.42	97.32	97.32	15.73
A,F	17	19:42:20	16	3.22	1.6×10^{-6}	152.8	20.0	0.63	110.72	110.72	89.56	89.56	33.09
A,F	17	19:56:30	9	3.23	8.2×10^{-7}	152.6	20.1	0.67	109.63	109.63	97.96	97.96	17.52
A,F	17	19:57:39	7	5.17	4.9×10^{-8}	155.8	22.7	0.67	109.87	109.87	100.97	100.97	13.09
A,F	17	20:03:56	13	3.23	1.3×10^{-6}	152.4	19.6	0.68	114.58	114.58	96.84	96.84	26.16
A,F	17	20:11:03	8	5.27	8.6×10^{-8}	149.7	20.3	0.72	99.15	99.15	88.40	88.40	14.94
A,F	17	20:18:15	5	4.37	2.0×10^{-7}	146.7	27.6	0.81	107.88	107.88	–	100.61	8.97
A,F	17	20:18:17	5	5.15	6.6×10^{-8}	152.7	18.9	0.70	109.20	109.20	–	103.10	8.76
A,F	17	20:24:49	19	1.48	4.6×10^{-6}	152.5	19.6	0.72	118.89	–	–	90.36	39.71
A,F	16	19:36:30	15	0.96	6.9×10^{-6}	152.3	22.0	0.64	109.80	109.80	89.08	89.08	32.54
A,F	16	19:43:50	15	1.83	3.1×10^{-6}	151.9	21.7	0.65	116.28	116.28	94.40	94.40	33.48
A,F	16	20:22:22	10	2.41	1.0×10^{-6}	153.0	21.1	0.72	113.69	113.69	99.46	99.46	19.93
A,F	16	20:35:47	5	–	–	154.0	20.6	0.73	108.68	108.68	101.47	101.47	9.87
A,F	16	20:36:27	17	1.71	4.0×10^{-6}	153.3	22.3	0.75	119.40	119.40	92.18	92.18	36.17
A,F	16	20:43:26	7	2.98	5.0×10^{-7}	153.1	20.5	0.75	111.67	111.67	101.74	101.74	13.26
A,F	16	20:48:29	8	3.01	5.8×10^{-7}	153.8	22.8	0.77	110.39	110.39	98.10	98.10	15.94
A,F	16	20:52:17	12	2.17	1.7×10^{-6}	153.6	22.1	0.77	113.60	113.60	94.00	94.00	25.25
J,K	17	21:10:20	17	–	–	155.2	21.5	0.79	122.99	122.99	95.21	95.21	34.67
J,K	17	21:21:58	28	–	–	153.9	21.6	0.82	137.96	137.96	85.96	85.96	62.81
J,K	17	21:26:36	12	–	–	153.5	22.8	0.84	116.48	116.48	94.76	94.76	25.72
J,K	17	19:17:47	13	–	–	153.4	21.9	0.59	112.11	112.11	–	94.60	29.25
J,K	17	19:29:03	14	–	–	153.0	21.8	0.62	120.37	120.37	–	100.54	31.64
J,K	17	19:36:12	12	–	–	153.0	21.4	0.63	118.43	118.43	–	101.15	26.94
J,K	17	20:02:44	15	–	–	153.7	21.5	0.68	120.47	120.47	97.16	97.16	32.98
J,K	17	20:25:16	17	–	–	153.7	21.5	0.73	116.73	116.73	89.10	89.10	37.13
J,K	16	19:33:11	22	–	–	152.6	22.5	0.63	144.43	144.43	110.66	110.66	52.29
J,K	16	19:35:00	18	–	–	152.9	22.7	0.63	112.01	112.01	86.22	86.22	39.79
J,K	16	20:31:37	16	–	–	153.2	22.1	0.74	116.85	116.85	90.75	90.75	34.22
J,K	16	20:36:11	21	–	–	153.3	21.8	0.75	127.91	127.91	91.11	91.11	48.35
J,K	16	20:59:05	25	–	–	153.1	21.9	0.79	130.91	130.91	87.07	87.07	54.85
A,F	17	22:01:18	14	0.77	4.2×10^{-6}	155.9	18.9	0.83	128.76	128.76	104.76	104.76	28.84
A,F	17	22:03:11	9	–	–	175.1	21.0	0.75	98.03	98.03	87.30	87.30	14.36
A,F	17	22:03:11	8	–	–	175.2	20.5	0.74	96.43	96.43	87.60	87.60	11.91
A,F	17	22:19:57	5	4.28	9.6×10^{-8}	155.1	19.9	0.86	108.76	108.76	101.21	101.21	8.74
A,F	18	21:07:56	5	5.13	4.4×10^{-8}	140.0	27.3	0.91	107.26	107.26	100.76	100.76	7.15
A,F	18	21:08:08	11	2.82	7.7×10^{-7}	173.2	14.6	0.60	110.38	110.38	97.62	97.62	21.42
A,F	18	21:12:45	18	1.51	9.3×10^{-6}	153.7	22.8	0.82	121.25	121.25	87.00	87.00	41.60
A,F	18	21:15:33	6	3.96	1.6×10^{-7}	150.5	38.8	0.93	105.80	105.80	98.16	98.16	8.19
A,F	18	21:23:23	5	3.62	1.9×10^{-7}	147.4	45.7	0.97	104.46	104.46	97.10	97.10	7.61
A,F	18	21:28:29	11	1.55	2.2×10^{-6}	153.4	25.0	0.86	121.11	121.11	99.98	99.98	24.53
A,F	18	21:48:39	9	3.70	2.4×10^{-7}	153.1	21.6	0.86	114.22	114.22	97.86	97.86	19.06
A,F	18	21:58:26	15	2.97	7.8×10^{-7}	166.1	–4.8	0.51	114.11	114.11	96.76	96.76	33.55
A,F	18	19:15:55	4	4.21	8.6×10^{-8}	170.5	10.2	0.29	116.25	116.25	114.92	114.92	4.61
A,F	18	20:14:33	12	4.59	1.2×10^{-7}	157.1	25.0	0.72	110.56	110.56	93.93	93.93	23.24
A,F	18	20:43:10	12	2.11	1.5×10^{-6}	157.2	26.4	0.78	111.19	111.19	91.95	91.95	24.64
A,F	17	19:23:39	8	5.48	6.1×10^{-8}	153.0	20.6	0.59	107.55	–	98.26	98.26	15.58
A,F	17	19:25:17	5	5.22	5.0×10^{-8}	156.6	15.8	0.52	112.45	112.45	–	108.09	8.56
A,F	17	19:29:46	5	6.05	1.5×10^{-8}	137.2	31.9	0.82	108.60	108.60	101.26	101.26	8.84
A,F	17	19:36:15	15	3.43	9.0×10^{-7}	153.1	19.4	0.61	119.35	119.35	–	100.76	30.57
A,F	17	19:39:56	19	3.11	1.3×10^{-6}	153.4	19.6	0.62	125.60	–	–	100.03	41.36
A,F	17	19:41:23	8	4.7	1.3×10^{-7}	152.2	20.4	0.64	107.42	–	97.19	97.19	15.73
A,F	17	19:42:20	16	3.22	1.6×10^{-6}	152.8	20.0	0.63	110.72	–	89.56	89.56	33.09
A,F	17	19:56:30	9	3.23	8.2×10^{-7}	152.6	20.1	0.67	109.63	109.63	97.86	97.86	17.52
A,F	17	19:57:39	7	4.12	1.7×10^{-7}	155.8	22.7	0.67	109.87	109.87	100.97	100.97	13.09
A,F	17	20:03:56	13	3.23	1.3×10^{-6}	152.4	19.6	0.68	114.58	114.58	96.76	96.76	26.16
A,F	17	20:11:03	8	5.27	8.6×10^{-8}	149.7	20.3	0.72	99.15	99.15	88.34	88.34	14.94
A,F	17	20:18:15	5	4.37	2.0×10^{-7}	146.7	27.6	0.81	107.88	107.88	–	100.61	8.97
A,F	17	20:18:17	5	5.15	6.6×10^{-8}	152.7	18.9	0.70	109.20	109.20	–	103.10	8.76
A,F	17	20:24:49	19	1.48	4.6×10^{-6}	152.5	19.6	0.72	118.89	–	–	90.36	39.71
A,F	17	21:06:47	6	4.23	7.2×10^{-8}	147.6	25.6	0.86	105.27	105.27	97.88	97.88	8.56

TABLE 1. *Continued*.

Cam	Day	Time (U.T.)	nf	Mag	Mass (kg)	RA	Dec	cos(*z*)	*Hf* (km)	*Hb* (km)	*He* (km)	*Hl* (km)	ΔL (km)
A,F	17	21:10:40	14	2.09	2.1×10^{-6}	154.3	19.5	0.78	115.27	115.27	93.66	93.66	27.57
A,F	17	21:11:11	11	2.17	1.5×10^{-6}	155.2	21.0	0.79	87.23	87.23	74.00	74.00	16.67
A,F	17	21:15:30	9	5.23	8.0×10^{-8}	155.3	20.5	0.79	110.73	110.73	96.34	96.34	18.10
A,F	17	21:30:12	17	1.77	2.8×10^{-6}	155.2	19.8	0.81	119.37	119.37	93.99	93.99	31.38
A,F	17	21:33:22	5	4.41	9.5×10^{-8}	154.5	26.9	0.87	98.63	98.63	91.49	91.49	8.21
A,F	17	21:35:20	23	0.22	1.2×10^{-5}	155.5	20.7	0.82	125.49	125.49	87.25	87.25	46.45
A,F	17	21:38:26	18	0.25	9.7×10^{-6}	154.9	20.6	0.83	117.36	117.36	87.87	87.87	35.57
A,F	17	21:38:39	5	4.52	1.2×10^{-7}	154.8	24.6	0.86	107.98	107.98	101.60	101.60	7.42
A,F	17	22:00:44	8	3.53	2.5×10^{-7}	154.9	19.7	0.84	115.77	115.77	102.46	102.46	15.80
A,F	17	21:46:28	7	3.62	2.9×10^{-7}	157.6	21.0	0.83	109.70	109.70	99.62	99.62	12.17
A,F	17	21:50:54	6	4.74	2.9×10^{-7}	141.3	22.0	0.89	105.24	105.24	96.14	96.14	10.16
A,F	17	21:51:02	7	4.23	1.1×10^{-7}	154.3	20.0	0.84	99.29	99.29	87.55	87.55	13.84
A,F	17	21:54:31	8	2.09	1.1×10^{-6}	–	–	0.83	114.89	114.89	102.01	102.01	15.57
A,F	17	21:56:55	8	3.84	2.3×10^{-7}	–	–	0.93	102.12	102.12	88.68	88.68	14.48

*Abbreviations: CAM = camera designations, Day = day (of November, 1998), Time = time (U.T.), nf = number of video frames, mag = apparent magnitude at maximum luminosity, mass = photometric mass (kg), RA = radiant right ascension, Dec = declination and error in degrees, cos(*z*) = cosine of zenith angle of trajectory, *Hf* = heights (first), *Hb* = Heights (beginning), *He* = heights (ending), *Hl* = heights (last), and ΔL = trail length (km). Where values were obtained with both cameras, only the value for the first camera is listed.

(1993). The local background is subtracted from each stellar or meteor image, and then the assumption is made that the logarithm of the summed pixel intensities in the bloomed image is approximately linearly related to the apparent visual magnitude. The standard luminosity equation (McKinley, 1961) is then used to determine photometric masses. It is assumed that the luminous efficiency factor depends linearly on velocity (as suggested by Whipple and reported in McKinley, 1961), and the value of the luminous efficiency factor as determined by Verniani (1965) was used in determining the photometric mass. It should be stressed that there is considerable uncertainty in the applicable luminous efficiency factor for fast meteors. Therefore, the absolute mass is uncertain, although this does not influence the relative mass of one meteor to another, or the shapes of the light curves.

RESULTS

Photometric Mass and Magnitude

For each double-station meteor, we averaged the various estimates of the photometric mass to obtain one mean value (we had potentially three values of photometric mass for some meteors: one from each station; and from one station, we had computed some masses using two slightly different digital image processing routines for the local background subtraction). The meteors ranged in astronomical magnitude from +0.25 to +6.05 with a mean value of +3.50. We provide in Fig. 2 a plot of astronomical magnitude at maximum luminosity *vs.* photometric mass for the wide field of view (cameras A and F) double-station Leonid meteors. For example, a 10^{-7} kg meteoroid corresponds to a peak luminosity of about +4.5 astronomical magnitudes.

TABLE 2. Parameters for the cameras for the double-station meteors reported in this paper.*

Id	Lens	Type	Loc	FOV	LM	Azim	Elev
A	25/0.85	Gen II	Obs	34.8×26.1	7.4	210	72
F	25/0.85	Gen II	Rem	33.2×24.9	7.8	17	79
J	50/0.95	Gen III	Obs	13.2×9.9	8.6	134	51
K	50/0.95	Gen III	Rem	13.7×10.2	8.7	97	51

*The first column gives an internal letter designation for the camera. The next column gives the focal length (in mm) and the F ratio of the objective lens. The image intensifier type is specified in the column labelled Type. Location (Loc) designates whether the camera was at the observatory (Obs) or the remote location (Rem). The field of view (FOV) is specified in degrees. LM refers to the apparent stellar limiting magnitude. Note that the limiting magnitude for Leonid meteors will be several magnitudes brighter than this value. Finally, the azimuth (Azim) and elevation (Elev) (both expressed in degrees) of the centre of the field of view are given in the last two columns.

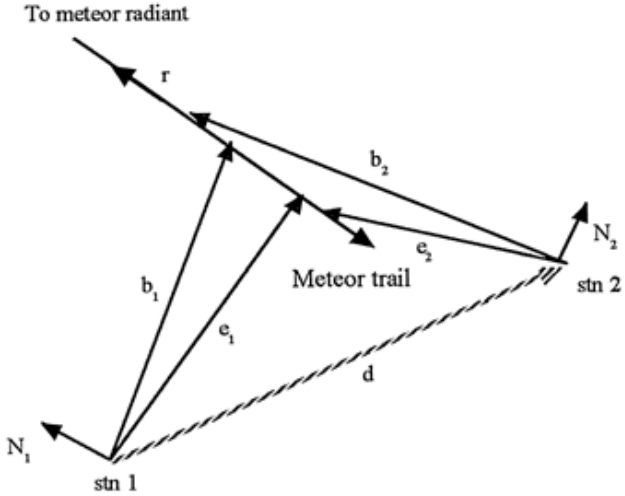

FIG. 1. Geometry used for the triangulation analysis. Vectors $\boldsymbol{b}_1$ and $\boldsymbol{e}_1$ point towards the apparent beginning and ending of the meteor as viewed from station 1 (and similarly from station 2). $\boldsymbol{N}_1$ and $\boldsymbol{N}_2$ represent normals to the planes containing the meteor as viewed from each station. The vector pointing towards the meteor radiant is $\boldsymbol{r}$.

We performed a regression fit of astronomical magnitude at maximum luminosity as a function of photometric mass (kg) and cosine of zenith angle, obtaining the following relationship:

$$M = -8.76\ (\pm 0.46) - 1.89\ (\pm 0.07) \log m_p - 1.35\ (\pm 0.63) \log \cos z$$

We can compare this with a similar relationship determined by Sarma and Jones (1985) on the basis of a study of 454 mainly sporadic meteors observed using image-intensified video detectors. After adjusting their regression to the Leonid velocity of 71.3 km/s and converting units to SI, we obtain the following fit from their work:

$$M = -9.45\ (\pm 0.36) - 2.02\ (\pm 0.15) \log m_p - 0.10\ (\pm 0.24) \log \cos z$$

Although there is some hint that the Leonid meteors have a slightly weaker dependence of magnitude on photometric mass, and a greater

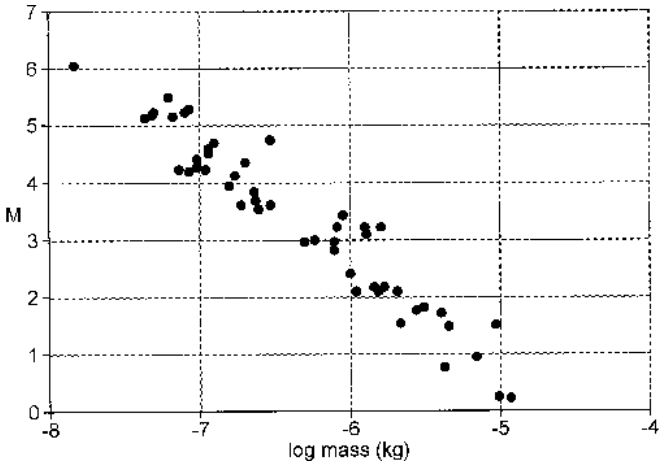

FIG. 2. Plot of logarithm of the astronomical magnitude at the brightest point on the meteor *vs.* the logarithm of the photometric mass (kg) for Leonid meteors observed by both cameras A and F.

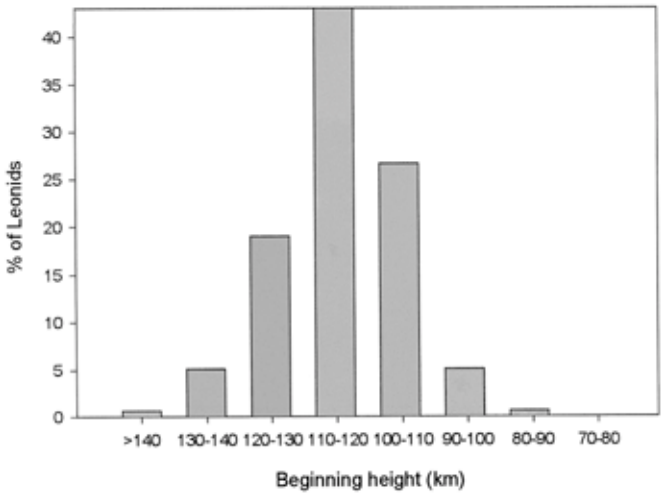

FIG. 3. Histogram of the distribution of beginning heights for the double-station Leonid meteors.

dependence of zenith angle, when the uncertainties in the parameters are considered the two distributions are essentially the same.

Heights

The sample of 79 double-station Leonid meteors produced accurate heights (with errors typically <2 km). The question of heights is of particular importance because of the proposed presence of organic compounds in meteors, with beginning heights providing the best indicator of chemical composition. In many cases, only part of the ablation profile of the meteor is within the field of view of the observing system. Thus, one must distinguish first heights from beginning true heights. In samples of true beginning heights, one has a bias against very low (and very high) meteors that are more likely to be excluded from the sample. In our sample, we found that the mean first height observed for the Leonid meteors was 113.0 km, the mean beginning height was 112.6 km, the mean ending height was 95.3 km, and the mean last height was 96.2 km. One must keep in mind that the samples are not the same—because a last height exists for every meteor, but only a portion of the data set has a true ending height.

We show in Fig. 3 a histogram of the percentage of the sample with beginning heights in various intervals. It can be seen that the vast majority of the observed double-station Leonid meteors begin in the interval from 100 to 120 km, and the highest beginning (and also first) height observed was 144.3 km for a meteor observed by the Generation III camera J at 19:33:11 U.T. on 1998 November 16. The paired camera K did not view the true beginning height for this meteor but recorded a first height of 138.75 km. Recent two-station observations have found Leonid meteors up to 160 km heights (*e.g.*, Fujiwara *et al.*, 1998) and higher (Betlem *et al.*, 1999). Note, however, that the largest mass Leonid meteoroids included in the present study sample was 1.2×10^{-5} kg, which is almost 3 orders of magnitude smaller than the Leonid meteoroids for which extreme beginning heights have previously been measured.

One possibility, however, is that the field-of-view overlap requirement for simultaneous observation from the two stations introduces a bias against extreme heights (Woodworth and Hawkes, 1996). The camera geometry had been designed so that the centre of the fields of view intersected at a height of 108 km. To evaluate this height bias, a numerical simulation was performed to determine height sensitivities. We calculated the percentage of meteors observed by one camera that would also be within the field of view of the other camera, using various trial meteor ablation heights. Although the fields of view (in terms of surface area covered) continue to rise with height, meteors at these heights would have their light diminished and the effective meteor rate would go down. Therefore, we applied a second correction on the basis of the diminished brightness because of the inverse square law loss of light intensity. To apply this correction, one must assume some mass distribution index for the shower, and we used a value of $s = 1.7$. In 1998, the s value varied extensively over the course of the shower, starting anomalously low ($s \approx 1.3$) on November 16, and then rising to a value in the range of 1.6 to 1.8 on Novmber 17 and 18. Arlt (1998) reports a value of $s = 1.36$ for November 16–17 and $s = 1.75$ on November 17–18. Murray *et al.* (1999) measured a value in the range of 1.44 to 1.67 on November 17–18 using similar equipment to that employed in this study. Small changes in s value would not dramatically affect the height bias simulations, and we assumed a constant value of $s = 1.7$ throughout.

Because of the large field of view of the A–F camera combination, and the high pointing elevation, there is not a severe height bias. Results of this simulation for the A–F camera combination are shown in Fig. 4. The curve marked "geometric" takes into consideration only the overlap at that height, whereas the curve marked "total" also takes into account the effect of loss of sensitivity at great heights. Although there is some bias against very high and low meteors (*e.g.*, 200 km Leonid meteors would only be detected with less than one-quarter the efficiency of Leonid meteors at 100 km), the tail of partial detection extends up to many hundreds of kilometers. Hence we may conclude that there is no absolute geometrical bias against reasonably high meteors. Although there may be occasional very high "tails" on the light curves of very bright Leonid meteors, as observed by Fujiwara *et al.* (1998), the beginning heights of most Leonid meteors are <145 km.

As well as the absolute value of the heights, a critical differentiating test for different models of dustball ablation is the way in which the heights vary with meteor magnitude or photometric mass. We show in Fig. 5 a plot of the first height for the double-station Leonid meteors observed with cameras A and F (wide field of view) *vs.* the astronomical magnitude at the brightest point on the meteor trajectory. There is relatively little dependence

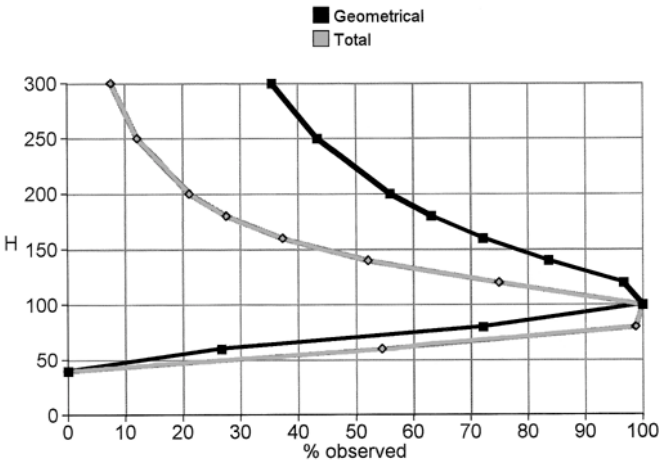

FIG. 4. The relative observational efficiency for meteors that ablate at different heights, for the geometry of the camera A–F pairing. The curve labeled geometric takes into account only the overlap between the two fields of view, whereas that labeled total also considers the effect of the meteor appearing fainter at greater heights.

of beginning height on meteor brightness. A regression of first height (km) with astronomical magnitude (at the brightest point on the meteor trail) yields the following relationship:

$$H_{\text{first}} = 123.9\ (\pm 1.7) - 3.0\ (\pm 0.4)\ M$$

Figure 6 is a similar plot, but for the last point observed for the meteor. Again, only meteors from the wide field of view systems (A, F) have been included, so as not to mix systems with significantly different fields of view and limiting sensitivities. A similar regression plot yielded the result:

$$H_{\text{last}} = 93.6\ (\pm 1.7) + 1.6\ (\pm 0.5)\ M$$

The fact that the heights are largely independent of meteor magnitude (and mass) is indicative of total clustering of the meteoroid into fundamental grains prior to the onset of intensive evaporation of the grains themselves (Hawkes and Jones, 1975; Campbell *et al.*, 1999). This is consistent with the relative absence of flares on all but the brightest of the Leonid meteors observed in 1998, and also with the findings for other shower meteors (Hapgood *et al.*, 1982; Beech, 1986; Campbell *et al.*, 1999).

Trail Lengths

Trail lengths were calculated for all two-station meteors. The trail length will depend principally on the zenith angle and on the

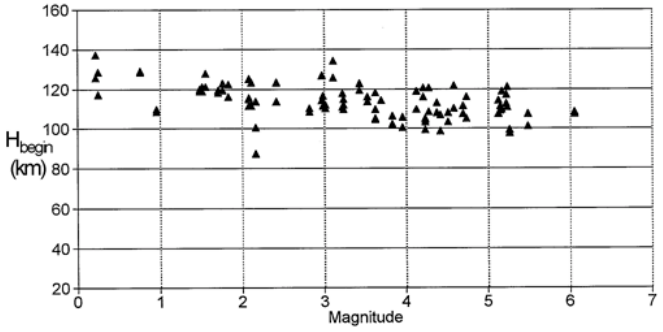

FIG. 5. A plot of the first height for the double-station Leonid meteors observed with cameras A and F (wide field of view) *vs.* the astronomical magnitude at the brightest point on the meteor trajectory. There is very little dependence of beginning height on meteor brightness.

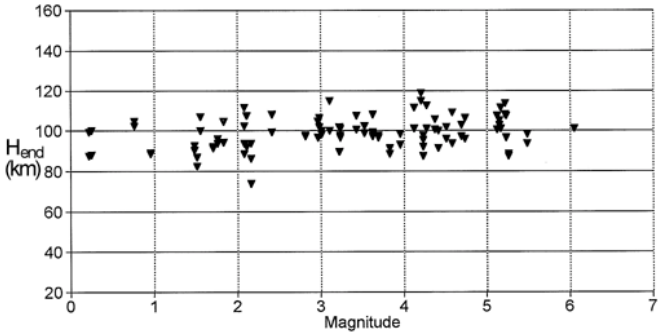

FIG. 6. A plot of the last height for the double-station Leonid meteors observed with cameras A and F (wide field of view) *vs.* the astronomical magnitude at the brightest point on the meteor trajectory. There is almost no dependence of ending height on meteor brightness.

mass of the meteor. Trail length, and its dependence on mass, provides an indicator of the physical characteristics of the meteor. Furthermore, knowledge of how trail length varies with mass is important for calibrating the effective collecting area of meteor radar systems. We performed a regression relating trail length (km) to these parameters (mass is expressed in kg), obtaining the result shown below.

$$dL = 110.5\ (\pm 7.1) - 12.5\ (\pm 5.4)\cos z + 12.8\ (\pm 0.9)\log m$$

There is a surprising amount of scatter on the zenith angle dependence. As expected, it is found that trail length will increase with increasing meteoroid mass and will decrease as the zenith angle is decreased. The fit suggests that a Leonid meteor with a zenith angle of 45.6° ($\cos z = 0.7$) and with a mass of 1.0×10^{-6} kg will have a trail length of 25.0 km, with a vertical trail length component of 17.5 km. A Leonid meteor with the same zenith angle but with a mass of 1.0×10^{-7} kg will have a trail length of 12.2 km. Caution should be exercised in applying this relationship, however, because the difference between the meteor magnitude and the limiting magnitude of the system will vary with meteor magnitude.

We plot in Fig. 7 trail length *vs.* meteor magnitude for the double-station Leonid meteors observed with cameras A and F. There is some hint of a flattening of the distribution below a mass of $\sim 1.0 \times 10^{-6}$ kg. The small size of the sample, the variety of zenith angles, and the differing amount that the meteors were above the limiting magnitude of the system all contribute to the large scatter in the distribution.

The fact that there is an increase in trail length with meteor mass is consistent with the dustball model of meteoroid ablation: small meteoroids are made up of grains of similar sizes, all of which take the same time and distance to ablate. Larger meteoroids either contain large grains, which ablate over a wider range of heights, or do not fragment completely before ablation. The final observed result should be a "flattening" in the trail length at smaller masses (as one approaches the limit at which individual grain ablation dominates the process) with a steeper dependence at large sizes where the meteoroid behaves more like a classical single body object—this is exactly what is observed.

Photometric Analysis

Light curves were obtained for 22 Leonid meteors with complete trails (*i.e.*, the full beginning and ending of the meteor was observed inside the camera field of view, and a number of photometric points were above the background by a statistically

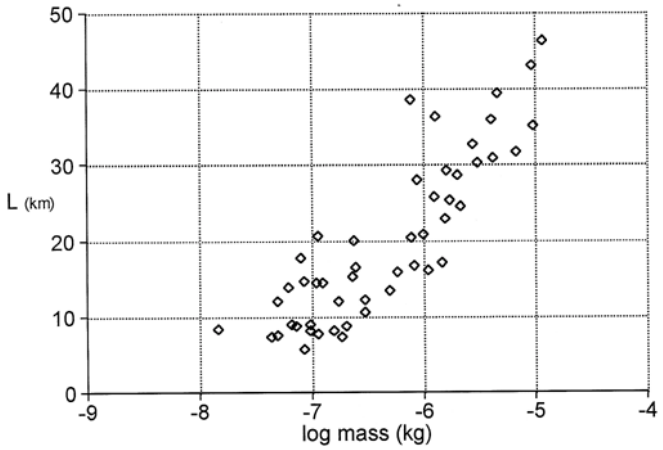

FIG. 7. Plot of trail length (km) *vs.* the logarithm of the photometric mass (kg). Although the trend of shorter trail length for fainter meteors predominates, there is a hint of a flattening of the curve for meteors smaller than 1.0×10^{-6} kg.

significant amount). As in our analysis of the 1997 Leonid meteors (Campbell *et al.*, 1998, 1999), shape parameters were obtained by fitting a parabola rotated by a certain angle (Campbell, 1998; Campbell *et al.* 1998). The coefficient of the second-order term of the parabola gives a measure of the width of the parabola: the angle of rotation defines the skew. This method has the advantage in that it uses all points on the curve to determine the two parameters, making it less susceptible to noise in the data than other methods. As with the 1997 Leonid meteors, the light curves were largely symmetric, with the average skew being slightly later than the midpoint. A histogram of skew values is provided in Fig. 8; the average skew and width of the curves are given in Table 3. Because a classically modelled single solid object has, in general, a wider, later skew light curve than those produced by Leonid meteors, the Leonid meteors observed in our TV sample are not solid, homogenous objects. A dustball model, in which each meteor is composed of a large number of tiny grains that ablate individually, can produce light curves of the kind observed (Campbell *et al.*, 1999).

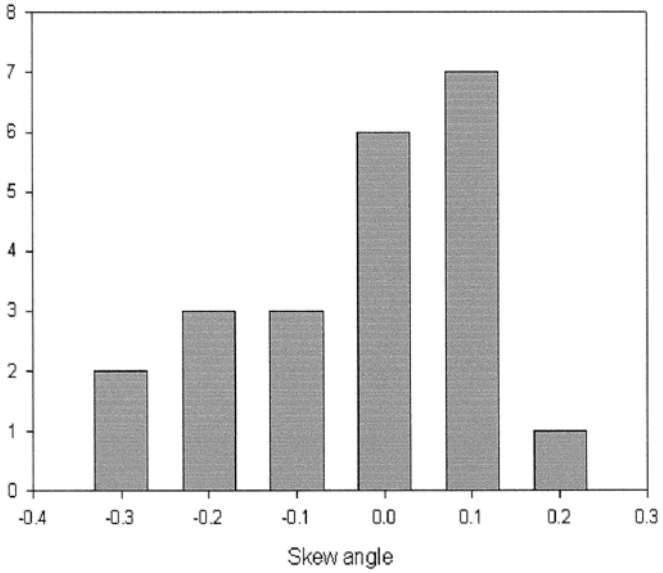

FIG. 8. Histogram of skew angle of meteor light curves. The majority of Leonid light curves are very close to symmetric (skew angle 0).

TABLE 3. Average results for the Leonid light curve fits.*

Angle	Width	Magnitude
–0.042 ± 0.124	8.42 ± 2.39	2.3

*Angle is a measure of the skew of the light curve. The average skew is symmetric, within the scatter of values. Width is a measure of the width of the ablation profile. Magnitude gives the average magnitude (at peak luminosity) of the 22 Leonid meteors that were used in this analysis.

No flares were observed on the vast majority of Leonid meteors recorded in 1998. Flares have only been observed on the very brightest meteors: this implies that small Leonid meteors have completely fragmented before they begin ablating. Larger Leonid meteors may still be in the process of breaking up during their luminous phase. This is also consistent with the results from 1997 (Campbell *et al.*, 1998; 1999), and with studies of other showers (Fleming *et al*., 1993).

ABLATION MODELS

The height of ablation is influenced by a number of factors, including the speed of the meteoroid, its mass, the heat required to ablate the meteor material, its boiling point, and the bulk density of the meteoroid. An earlier modeling process that was used to estimate the ablation of Leonid meteoroids (Campbell *et al.*, 1999; Fyfe and Hawkes, 1986) was modified to include particles of different chemical compositions. In particular, maximum beginning heights and minimum ending heights were found for Leonid meteors over the complete observed size range. Three different bulk compositions were investigated: stony (similar to chondritic meteorites), density of 3500 kg/m^3 and a melting point of 2100 K; Fe, density of 7650 kg/m^3 and melting point of 3000 K; and a complex organic $C_{18}H_{34}O_4$, density of 1500 kg/m^3 and melting point of 600 K. More volatile substances, like water, have little chance of surviving the Sun's heat at the Earth's distance from the Sun, and the latter organic was suggested by Elford *et al.* (1997) to be one of the simplest compounds stable enough to last more than one passage around the Sun. We show the results of these simulations in Table 4. A dustball meteoroid made of only any one of these substances could conceivably produce luminosity over the complete range of heights given for that substance in Table 4 (depending on the distribution of grain sizes) but could not be observed higher or lower than this.

From our simulations of ablating Leonid meteors, Fe begins ablating at a maximum height of 109 km. Because 73% of the meteors had initial heights greater than this, Fe is not likely a major component of Leonid meteoroids. Solid stone, which was used in modeling Leonid TV observations from 1997, begins ablating at a maximum height of 118 km. Again, a significant number (34%) of the precision results give heights higher than this. Our chosen complex organic compound ablated between 163 and 121 km.

Although this would seem to suggest that many of the Leonid meteoroids have significant organic inclusions, this is not necessarily the case. Other compounds, or physical structures, might produce heights that also fit the data; notably, porous stone having a lower density than that assumed, but otherwise similar characteristics. More volatile metals, such as Na, would also ablate higher than stone or Fe. Indeed, differential ablation of Na has been observed in the spectrum of TV Leonid meteors (Borovicka *et al.*, 1999), and this suggests that Na composes some of the volatile "glue" holding the meteoroid together. Additional evidence for differential ablation in Leonid meteors has been obtained with multifrequency lidar

TABLE 4. Maximum and minimum ablation heights for Leonid meteoroids assumed to have a dustball physical structure for three different assumed compositions.

Substance	Highest beginning height (km)	Lowest ending height (km)
Fe	109	95
Stone	118	99
$C_{18}H_{34}O_4$	163	121

systems (von Zahn *et al.*, 1999). If Leonid meteoroids were largely organic, it would mean that their masses are much larger than calculated, because the luminous efficiency depends on chemical composition. Carbon radiates predominantly in the ultraviolet, which is not recorded on the intensified video, whereas chondritic-like substances and metals radiate extensively in the visible and would produce more total light from less initial mass. Spectral information would be required to further narrow down the composition: a spectral camera was used in the 1999 Leonid campaign, the results of which have not yet been analysed.

DISCUSSION AND CONCLUSIONS

The heights which we have measured are consistent with those reported in Betlem *et al*. (1999) from photographic observations of the 1998 Leonid shower. The shapes of the light curves are consistent with our earlier measurements (Campbell *et al.*, 1999) and with other observations of the 1998 Leonid shower (Murray *et al.*, 1999). Overall, the dependence of magnitude on photometric mass, the heights of ablation, and the trail lengths are similar to those reported for sporadic meteors and the Perseids (Hawkes and Jones, 1980; Hawkes *et al*., 1984; Sarma and Jones, 1985; Ueda and Fujiwara, 1995).

We have not found evidence for anomalously high Leonid meteors, as reported by Fujiwara *et al.* (1998), although, as noted earlier, the meteors studied here are not nearly as bright as those with anomalous heights. It is possibly significant that our highest beginning heights were registered with the Generation III cameras, possibly indicating either that there is a long, low luminosity early portion of the ablation light curves that was detected by these more sensitive cameras, or that the early trail emits mainly in the red and infrared and was therefore more effectively imaged by the Generation III systems.

The trail lengths and light curves of the Leonid meteors studied here are broadly consistent with the two-component dustball model of meteor ablation (Hawkes and Jones, 1975). The lack of significant flares on small meteors implies that little fragmentation takes place once ablation begins, and the symmetry of the light curves is consistent with a large number of small grains. In some cases, non-atmospheric processes may be responsible for the fragmentation of meteoroids. We feel that the "outburst" observed in the 1997 Leonid shower by Kinoshita *et al*. (1999) may be an example of a Leonid meteoroid that clustered in interplanetary space. A less spectacular cluster was observed by Piers and Hawkes (1993) for a non-Leonid meteor. In at least two examples from the 1998 Leonid meteors, we observed significant transverse spread in the light production region, indicative of a severely fragmented dustball meteoroid (LeBlanc *et al*., 2000).

The beginning heights of the Leonid meteors reported here are higher than can be explained with the ablation of solid stone, unless the structure is unusually porous with a very low bulk density. Possible candidates for light at these altitudes include heavy organic compounds, Na or other volatile metals, and porous stone. If the meteors are primarily organic, it would mean that the luminous efficiency is much lower, and therefore the masses much higher than those calculated using classical meteor ablation. Metals, on the other hand, would tend to have a greater luminous efficiency and therefore lower masses. Spectral information, particularly in the infrared and ultraviolet, would be useful for narrowing down the range of possible substances.

Clearly additional observations, particularly those that combine two-station triangulation for precise heights, spectroscopy, and precise determination of light curves, are needed to more fully specify the physical structure and chemical composition of Leonid meteoroids. Also, clearly it is necessary to make more sophisticated ablation models, which take into account a mixed chemical composition and which have more sophisticated modeling of the thermal processes.

Acknowledgements–The Leonid 98 campaign was funded by the U.S. Air Force, National Aeronautics and Space Administration, National Reconnaissance Office, Canadian Space Agency, European Space Agency, CRESTech, Department of National Defense, and Defense Research Establishment Ottawa. Positional and photometric analysis software was written by I. S. Murray, who also contributed, performed primary measurements, and analysis on a portion of the data reported here. Meteor detection software written by Pete Gural was used to find Leonid meteors on video. Martin Connors, Alan Hildebrand, Tiffany Montague, Barry Tilton, and Pete Gural helped with data collection. Research Grants to Mount Allison University and the University of Western Ontario from the Natural Sciences and Engineering Research Council of Canada supported some aspects of this work.

Editorial handling: S. Sandford

REFERENCES

ARLT R. (1998) Bulletin 13 of the International Leonid Watch. *WGN J. Inter. Meteor Org.* **26,** 239–248.

BEECH M. (1984) The structure of meteoroids. *Mon. Not. R. Astron. Soc.* **211,** 617–620.

BEECH M. (1986) The Draconid meteoroids. *Astron. J.* **91,** 159–162.

BETLEM H. ET AL. (1999) Very precise orbits of 1998 Leonid meteors. *Meteorit. Planet. Sci.* **34,** 979–986.

BOROVICKA J., STORK R. AND BOCEK J. (1999) First results from video spectroscopy of 1998 Leonid meteors. *Meteorit. Planet. Sci.* **34,** 987–994.

CAMPBELL M. D. (1998) Light Curves of Faint Meteors: Implications for Physical Structure. B.Sc. honours thesis, Mount Allison University. 102 pp.

CAMPBELL M. D., HAWKES R. L. AND BABCOCK D. D. (1998) *Leonid Light Curves and Implications for Physical Structure*. 31 July 1998 CRESTech Contract Report. 32 pp.

CAMPBELL M. D., HAWKES R. L. AND BABCOCK D. D. (1999) Light curves of faint shower meteors: Implications for physical structure. In *Meteoroids 1998* (eds. V. Porubcan and W.J. Baggaley), pp. 363–366.

CEPLECHA Z. (1987) Geometric, dynamic, orbital and photometric data on meteoroids from photographic fireball networks. *Bull. Astron. Inst. Czechosl.* **38,** 222–234.

CEPLECHA Z., SPURNY P., BOROVICKA J. AND KECLIKOVA J. (1993) Atmospheric fragmentation of meteoroids. *Astron. Astrophys.* **279,** 615–626.

CEPLECHA Z., BOROVICKA J., ELFORD G. W., REVELLE D., HAWKES R., PORUBCAN V. AND SIMEK M. (1998) Meteor Phenomena and Bodies. *Space Sci. Rev.* **84,** 327–471.

CORRELL R. R., CAMPBELL M., LEBLANC A., WORDEN S. P., HAWKES R. L., MONTAGUE T. AND BROWN P. (1999) Electro-optical observational results of the 1998 Leonid shower. In *Leonid Meteoroid Storm and Satellite Threat Conference* (eds. D.K. Lynch and W. H. Ailor), Aerospace Corp., Los Angeles, California, USA

ELFORD W., STEEL D. AND TAYLOR A. (1997) Implications for meteoroid chemistry from height distribution of radar meteors. *Adv. Space Res.* **20,** 1501–1504.

FISHER A. A., HAWKES R. L., MURRAY I. S., CAMPBELL M. D. AND LEBLANC A. G. (2000) Are meteoroids really dustballs? *Planet. Space Sci.* **48,** 911–920.

FLEMING D. E. B., HAWKES R. L. AND JONES J. (1993) Light curves of faint television meteors. In *Meteoroids and Their Parent Bodies* (eds. J. Stohl and I. P. Williams), pp. 261–264. Astronomical Institute of the Slovak Academy of Science.

FUJIWARA V., UEDA M., SHIBA Y., SUGIMOTO M., KINOSHITA M., SHIMODA C. AND NAKAMURA, T. (1998) Meteor luminosity at 160 km altitude from TV observations for bright Leonid meteors. *Geophys. Res. Lett*. **25,** 285–288.

FYFE J. D. D. AND HAWKES R. L. (1986) Residual mass from ablation of meteoroid grains detached during atmospheric flight. *Planet. Space Sci*. **34**, 1201–1212.

HAPGOOD M., ROTHWELL P. and ROYVRIK O. (1982) Two station observations of Perseid meteors. *Mon. Not. R. Astron. Soc.* **201,** 569–577.

HAWKES R. L. AND JONES J. (1975) A quantitative model for the ablation of dustball meteors. *Mon. Not. R. Astron. Soc.* **173,** 339–356.

HAWKES R. L. AND JONES J. (1980) Two station television meteor studies. In *Solid Particles in the Solar System* (eds. I. Halliday and B. A. McIntosh), pp. 117–120. D. Reidel Publishing Company, Dordrecht, The Netherlands.

HAWKES R. L., JONES J. AND CEPLECHA Z. (1984) The populations and orbits of double-station TV meteors. *Bull. Astron. Inst. Czechosl.* **35,** 46–64.

HAWKES R. L., MASON K. I., FLEMING D. E. B. AND STULTZ C. T. (1993) Analysis Procedures for Two Station Television Meteors. In *International Meteor Conference 1992* (eds. D. Ocenas and D. Zimnikoval), pp. 28–43. International Meteor Organization, Antwerp, Belgium.

HAWKES R. L., CAMPBELL M. D., BABCOCK D. D. AND BROWN P. (1998) observations. In *Leonid Meteoroid Storm and Satellite Threat Conference* (eds. D. K. Lynch and W. H. Ailor), Aerospace Corp., Los Angeles, California, USA.

JACCHIA L. G. (1955) The physical theory of meteors VIII: Fragmentation as cause of the faint-meteor anomaly. *Astrophys. J.* **121,** 521–527.

KINOSHITA M., MARUYAMA T. AND SAGAYAMA T. (1999) Preliminary activity of Leonid meteor storm observed with a video camera in 1997. *Geophys. Res. Lett*. **26,** 41–44.

LEBLANC A. G. ET AL. (2000) Evidence for transverse spread in Leonid meteors. *Mon. Not. R. Astron. Soc.* **313,** L9–L13.

MARSDEN B. G. (1982) How to reduce plate measurements. *Sky Telescope* **64,** 284.

MCKINLEY D. W. R. (1961) *Meteor Science and Engineering.* McGraw-Hill, New York, New York, USA. 309 pp.

MURRAY I. S., HAWKES R. L. AND JENNISKENS P. (1999) Airborne intensified charged-coupled device observations of the 1998 Leonid shower. *Meteorit. Planet. Sci*. **34,** 949–958.

ÖPIK E. (1958) *Meteor Flight in the Atmosphere.* Interscience Publishers, London, U.K.

PIERS P. A. AND HAWKES R. L. (1993) An unusual meteor cluster observed by image intensified video. *WGN J. Inter. Meteor Org*. **21,** 168–174.

SARMA T. AND JONES J. (1985) Double-station observations of 454 TV meteors—I. Trajectories. *Bull. Astron. Inst. Czechosl*. **36,** 9–24.

SHADBOLT L. AND HAWKES R. L. (1995) Absence of wake in faint television meteors. *Earth Moon Planets* **68,** 493–502.

STEEL D. (1998) The Leonid meteors: Compositions and consequences. *Astron. Geophys* **39,** 24–26.

UEDA M. AND FUJIWARA Y. (1995) Television meteor radiant mapping. *Earth Moon Planets* **68,** 585–603.

VERNIANI F. (1965) On the luminous efficiency of meteors. *Smithson. Contr. Astrophys.* **9,** 141–172.

VERNIANI F. (1969) Structure and fragmentation of meteoroids. *Space Sci. Rev*. **10,** 230–261.

VON ZAHN U., GERDING M., HOFFNER J., MCNEIL W. J. AND MURAD E. (1999) Iron, calcium and potassium atom densities in the trails of Leonids and other meteors: Strong evidence for differential ablation. *Meteorit. Planet. Sci.* **34,** 1017–1027.

WOODWORTH S. C. AND HAWKES R. L. (1996) Optical search for high meteors in hyperbolic orbit. *Astron. Soc. Pacific Conf. Series* **104,** 83–86.

WRAY J. D. (1967) *The Computation of Orbits of Doubly Photographed Meteors.* Univ. New Mexico Press, Albuquerque, New Mexico, USA. 211 pp.

Forward

Back

Table of Contents